Available at www.sciencedirect.com

ScienceDirect

journal homepage: www.elsevier.com/locate/issn/15375110

Research Paper

# Intelligent multi-sensor system for the detection and treatment of fungal diseases in arable crops

D. Moshou [a,*], C. Bravo [b], R. Oberti [c], J.S. West [d], H. Ramon [b], S. Vougioukas [a], D. Bochtis [e]

[a] Aristotle University of Thessaloniki, Agricultural Engineering Lab, Faculty of Agriculture, P.O. 275, 54124 Thessaloniki, Greece
[b] Division of Mechatronics, Biostatistics and Sensors, Department of Biosystems, K.U. Leuven, Belgium
[c] Istituto Di Ingegneria Agraria, Universita Degli Studi di Milano, Italy
[d] Plant Pathology and Microbiology Department, Rothamsted Research, Harpenden AL5 2JQ, UK
[e] University of Aarhus, Faculty of Agricultural Sciences, Department of Biosystems Engineering, Blichers Allé 20, 8830 Tjele, Denmark

ARTICLE INFO

*Article history:*
Received 17 August 2010
Received in revised form
7 December 2010
Accepted 8 January 2011
Published online 16 February 2011

The development of a ground-based real-time remote sensing system that can be carried by tractors or robotic platforms is described. This prototype system makes possible the detection of plant diseases in arable crops automatically at an early stage of disease development and during field operations. The methodology uses differences in reflectance between healthy and diseased plants. Hyperspectral reflectance and multi-spectral imaging techniques were developed for simultaneous acquisition in the same canopy. Experimental platforms were constructed, and the advantage of using sensor fusion was demonstrated. An intelligent multi-sensor fusion decision system based on neural networks was developed to predict the presence of diseases or plant stresses, in order to treat the diseases in a spatially variable way. A robust multi-sensor platform integrating optical sensing, GPS (Geostationary Positioning System) and a data processing unit was constructed and calibrated. The functionality of automatic disease sensing and detection devices is crucial in order to conceive a site-specific spraying strategy against fungal foliar diseases. Field tests were carried out to optimise the functioning of the multi-sensor disease detection device. An overview is provided on how disease presence data are processed in order to enable an automatic site-specific spraying strategy in winter wheat. Furthermore, mapping of diseases based on automated optical sensing and intelligent prediction provide a spatially variable recommendation for spraying.



## 1. Introduction

In order to reduce the amounts of fungicides sprayed on wheat fields, a new approach has been developed. This method seeks to apply fungicides according to the required dose, which can be determined based on the health status of the wheat plants. This implies spraying less or no fungicide on healthy parts of the field, while infected parts should be fully covered. The advantage would be double: less environmental loading by chemicals and reduced spraying costs for the field operator.

There are strong indications that plant diseases can be detected automatically. The carriers of information for detection considered in this paper are electromagnetic waves.

* Corresponding author.
E-mail address: dmoshou@agro.auth.gr (D. Moshou).
1537-5110/$ – see front matter © 2011 IAgrE. Published by Elsevier Ltd. All rights reserved.
doi:10.1016/j.biosystemseng.2011.01.003

**Nomenclature**

$I_{675}(x,y)$ monochromatic sub-image where (x,y) represent pixel coordinates
$I_{750}(x,y)$ monochromatic sub-image where (x,y) represent pixel coordinates
$I_{NDVI}(x,y)$ normalised difference vegetation image where (x,y) represent pixel coordinates
$n_H$ number of pixels corresponding to healthy tissue
$n_L$ number of pixels corresponding to lesions

*Abbreviations*

| | |
|---|---|
| ARI | Anthocyanin Reflectance Index |
| CCD | Charge Coupled Device |
| CIR | Colour Infrared |
| COV | Circle of View |
| DGPS | Differential Geostationary Positioning System |
| DSS | Decision Support System |
| FOIS | Fibre Optic Imaging Spectrograph |
| FOV | Field of View |
| GLD | Grapevine Leafroll Disease |
| QDA | Quadratic Discriminant Analysis |
| LI | Lesion Index |
| LIS | Line Imaging Spectrograph |
| LOV | Line of View |
| MLP | Multi-Layer Perceptron |
| NIR | Near-infrared |
| NN | Neural Network |
| PRI | Photochemical Reflectance Index |
| RGB | Red Green Blue |
| SWIR | Short Wave Infrared |
| SWNIR | Short Wave Near-infrared |
| TCARI | Transformed Chlorophyll Absorption and Reflectance Index |
| VIS | Visible spectrum |

The hypothesis is that healthy plants interact (absorb, reflect, emit, transmit or fluoresce) with electromagnetic radiation differently from infected plants. Plants show different optical properties. Some of them can be seen by the naked eye, others are revealed using advanced equipment. Light reflection measurement techniques are very helpful for detecting these properties. These comprise spectral measurements, where an overall average measurement of light quality in visible and/or other wavebands is determined from a field of view, or imagery, and where the quality of light from individual pixels forming an image of the field of view is used to classify healthy and diseased tissues. According to Lee et al. (2010), at the earliest infection stages fluorescence is the most appropriate technique for fungal disease detection since it samples the health status in terms of photosynthetic efficiency. Fluorescence alone cannot provide a clear indication of specific stress factors, having only medium detection accuracy, while accuracy is sensitive to light intensity.

Following the initial metabolic changes, the fungus spreads radially around its infection point. The initial infection area necroses: it loses pigmentation, the photosynthetic apparatus is disassembled and the cell walls collapse. At this moment infection patterns become visible. According to Lee et al. (2010), analysis of the light reflection can help in detecting infection from this stage onwards. Pathogen propagules can be detected in the visible spectrum (400–700 nm) depending on the pathogen; chlorophyll degradation in the visible spectrum and red-edge; senescence in the visible spectrum and short wave near-infrared (680–800 nm) due to browning and near-infrared (1400–1600 nm and 1900–2100 nm) due to dryness; changes in canopy density and leaf area in the short wave near-infrared.

Multispectral imagery is created by sensors that measure reflected light within several bands of the electromagnetic spectrum. Multispectral sensors usually have between 3 and 10 different band measurements in each pixel of the images they produce. Hyperspectral sensors measure energy in narrower and more numerous bands than multi-spectral sensors. Hyperspectral images can contain as many as 200 (or more) contiguous spectral bands. The numerous narrow bands of hyperspectral sensors provide a continuous spectral measurement across the entire electromagnetic spectrum and therefore are more sensitive to subtle variations in reflected energy. In the case of disease detection, multi-spectral imaging can provide an estimate of the spatial pattern of disease lesions while hyperspectral imaging can provide line spectrography.

The disease will gradually take control of the entire plant, which will show a global stress leading to a general closure of the stomata, in order to reduce water losses. This change in transpiration can be monitored by thermography. However, the overall leaf temperatures change rapidly, and are heavily dependent upon ambient temperature, illumination and wind. Therefore, due to changing environmental factors, thermography gives poor results when used on proximal sensing platforms.

Taking into account the relative advantages and disadvantages of the different sensing techniques, a combination of spectral techniques is clearly advantageous due to higher recognition accuracy and less sensitivity to environmental factors. According to Lee et al. (2010), fluorescence sensing achieves medium detection accuracy and is sensitive to light intensity. Disease detection based on thermography is highly dependent on illumination, has very low accuracy in changing weather conditions and is sensitive to leaf coverage.

Disease detection based on spectral reflection information relies on the properties of the light emerging from the canopy after multiple interactions, i.e. reflection, transmission and absorption, with the tissues of the plant. This diffusely reflected radiation forms the canopy spectral signature, a function described by the ratio of the intensity of reflected light to the illuminated light for each wavelength in the visible region (400–700 nm), the short wave near-infrared region (700–1100 nm) and the near-infrared region (1100–2500 nm). Leaf reflectance is defined as the proportion of the irradiated light reflected by the leaf.

Diseases can affect the optical properties of leaves at many wavelengths, thus disease detection systems may be based on

spectral measurements in different wavebands or a combination of wavebands. Healthy plants appear green since the green light band (ca. 550 nm) is reflected relatively efficiently compared to blue, yellow and red bands, which are absorbed by photoactive pigments. Diseased plants usually exhibit discrete lesions on leaves, corresponding to necrotic or chlorotic regions, which increase reflectance in the VIS (Visible Spectrum) range, especially in the chlorophyll absorption bands. In particular, reflectance changes at wavelengths around 670 nm, cause the red-edge (the sharp transition in the reflectance spectrum from low VIS reflectance to high NIR (Near-infrared) reflectance that generally occurs around 730 nm) to shift to shorter wavelengths. Conversely, biomass reduction linked to senescence, reduced growth and defoliation, decreases the canopy reflectance in the NIR band. Following detection of stress in tomatoes induced by late blight disease, Zhang, Qin, Liu, and Ustin (2003) determined that the spectral reflectance in the NIR region, especially at 0.7–1.3 μm, was much more valuable than the visible range to detect many crop diseases. Muhammed and Larsolle (2003) concluded that the fungus *Drechslera tritici-repentis* mainly affected the spectral signature by (1) a flattening of the green reflectance peak together with a general decrease in reflectance in the near-infrared region and (2) a decrease at the shoulder of the near-infrared reflectance plateau together with a general increase in the visible region between 550 and 750 nm.

Devadas, Lamb, Simpfendorfer, and Backhouse (2009) concluded that, in order to discriminate between different wheat rust species, there was a need to use a combination of different spectral indices as it was impossible to achieve high discrimination performance by using isolated indices. A sequential application of firstly the Anthocyanin Reflectance Index (ARI) to separate healthy, yellow rust and mixed stem rust/leaf rust classes followed by the Transformed Chlorophyll Absorption and Reflectance Index (TCARI) to separate leaf and stem rust classes could provide a means of wheat rust species discrimination. Huang et al. (2007) showed that the Photochemical Reflectance Index (PRI) was a very robust spectral index for quantifying yellow rust infection. The effectiveness of PRI was explained by the fact that it is highly correlated to biomass and foliar nitrogen content, with which rust incidence is generally negatively correlated. An important result regarding early detection of viral diseases is presented in Naidu, Perry, Pierce, and Mekuria (2009) who showed that it is possible to detect the presence of grapevine leafroll disease (GLD) even at a pre-symptomatic stage. This was mainly due to the negative effect of the virus infection on the physiology of the plant resulting in metabolic and pigment changes.

Typically, RGB-images represent a red, green and blue waveband, similar to human vision. Other waveband images can be acquired, e.g. with a colour infrared (CIR) camera. This provides multi-spectral images with some true-colour sensitive wavebands, as well as an NIR waveband. Representation is possible using separate black–white images or false colour images. The effectiveness of disease detection depends on the data processing algorithms that are used. For each crop-disease system, spectroscopy imaging methods can be used to simplify and automate disease detection. An important step involves the generation and selection of appropriate features that are sensitive to the presence of disease. Signal processing can be used to generate spectral features that increase classification performance, while maintaining immunity against disturbing factors like noise, and are robust against variability in environmental conditions. For example, Moshou, Bravo, West, McCartney, and Ramon (2004), and Bravo, Moshou, West, McCartney, and Ramon (2003) used image analysis algorithms to discriminate between background and wheat canopy (based on reflectance at 675 nm and 750 nm) and then by classification of combinations of spectral wavebands to discriminate between healthy leaf tissue and yellow rust disease lesions in winter wheat (West et al., 2003). Further improvement resulted from multi-sensor fusion of spectral and fluorescence features (Moshou, Bravo, Oberti et al., 2005) where a spectrograph provided a combination of reflectance intensities at selected wavebands. In the same paper, these data were combined with lesion indices resulting from fluorescence imaging of the same plants.

Previous work on wheat yellow rust detection has been based on single sensors or fusion of sensor data. Examples include the work of Zhang and Dickinson (2001), where fluorescence is used to assess the dynamics of fungal growth in wheat. Another approach presented by Bravo, Moshou, West et al. (2003) concerns the detection of yellow rust in wheat by using spectral information from a spectrograph. This approach was extended to include the use of neural networks in order to increase the detection performance (Moshou, Bravo, West et al., 2004). The advantage of using sensor fusion of spectral and fluorescence imaging features has been shown by Moshou, Bravo, Oberti et al. (2005). Image processing methods to detect soybean rust from multi-spectral images under laboratory conditions have been presented by Cui, Zhang, Li, Hartman, and Zhao (2010).

One disadvantage with previous work is that the methods developed sensors that were not specifically designed and constructed for use on a spraying machine. Some sensors are difficult to implement practically on a sprayer due to the requirements that the sensors impose, e.g. dark adaptation in the case of fluorescence imaging. The approach proposed here concentrates on developing a tractor-mounted sensor based on infrared spectroscopy and multi-spectral imaging, which can provide complementary information about yellow rust presence. Moreover, the whole system has been designed to detect and map disease presence on-line as the tractor traverses the field.

An additional objective of this work is to propose a site-specific spraying strategy against fungal foliar diseases in winter wheat. This strategy depends upon the ability to detect diseases accurately. However, automatic disease sensing devices are limited in their capacity to detect infestations in the field. This paper reviews the reason why and considers how the infestation stage of fungal diseases can be detected. Finally, taking into account the limitations of automatic disease sensing, an overview is provided on how this information can be used for spraying efficiently against foliar fungal diseases. The diseases under investigation were yellow rust (pathogen *Puccinia striiformis*) and septoria leaf blotch (pathogen *Septoria tritici*).

## 2. Materials and methods

### 2.1. Field experiments

A field trial was especially designed to cross both diseases (septoria leaf blotch and yellow rust) with nitrogen stresses, and established on land owned by the "Centre Alphonse De Marbaix" of UCL at Louvain-la-Neuve to test the prototype platform in its final optimised configuration. A 56 × 220 $m^2$ area, sown on 24 November 2002 with the wheat cultivar Baltimor, which is very susceptible to infection by both pathogens *P. striiformis* and *S. tritici*, was divided into three randomised blocks. In each block, three different fertilisation levels were crossed with three different disease treatments on nine different plots (Fig. 1).

The controls and buffer zones were sprayed on 7 May 2003 with a combination of OPERA (epoxiconazole and pyraclostrobine) 1.5 l $ha^{-1}$ and IMPULSE (Spiroxamine) 1.5 l $ha^{-1}$. A second application was made on 16 June with OPERA (1.5 l $ha^{-1}$) only. Insecticide Keschet was sprayed on 4 May against Lema (*Oulema melanopus Linné*). The recommended fertiliser doses for the field were 80–140 kg $ha^{-1}$ of N, 50 P and 113 K (based on soil analysis performed by the "UCL-laboratoire d"écologie des prairies" at Michamps). Three application dates were planned: at tillering, at stem elongation and at ear emergence. The first application was made on 25 March 2003 with an NPK mixture (14-10-24). The medium level received close to the recommended dose while the high and the low level received 50% more and 50% less than this dose respectively. These three fertilisation levels were crossed with two diseases (yellow rust and septoria leaf blotch) and a healthy control (non-inoculated) treatment giving 9 different conditions per block (Fig. 1). The two diseases were inoculated by means of pots containing infected plants. For yellow rust 18 pots containing 10 seedlings were inoculated on 11 March in controlled conditions with *P. striiformis* strain 233E137v17. One set of 9 pots was placed on the field on 14 March. A second set was placed on 27 March after a longer stay into the greenhouse at 14–16 °C, 16 h photoperiod. The first sporulation started outside on 28th March and continued for more than four weeks. For septoria leaf blotch, naturally infected plants were transplanted on 24 March from a wheat field located at Louvain-la-Neuve, Bruyère2, to our field. Five tillers showing leaf necrosis containing *S. tritici* pycnidia were placed at two metres right from the centre of each of the 9 plots reserved for *S. tritici* treatments.

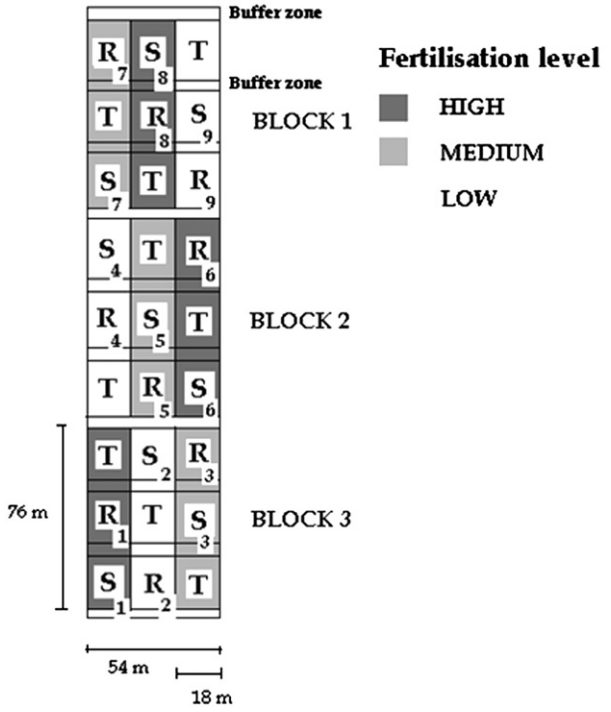


**Fig. 1 – Field trial at Louvain-la-Neuve, growing season 2002–2003. Effect of the two diseases yellow rust and septoria leaf blotch crossed with three different fertilisation levels. Three repetitions (blocks 1–3) and nine plots/repetition. Plots R4, R7 and R8 have been used for evaluating the yellow rust detection capability of the multisensor prototype. The following conventions have been used regarding disease and fungicide spraying: T: fungicide protected control, R: *P. striiformis* inoculation, S: *S. tritici* inoculation.**

The different levels of nitrogen fertilisation were included in the experiments because they affect the optical characteristics of the diseased plants. The inclusion of different fertilisation levels crossed with the two diseases tests the robustness of the classifier against variations due to different nitrogen content. The disease prototype has been tested only in the case of yellow rust because it appeared in patches and therefore allowed topical treatment. On the other hand, septoria leaf blotch appeared to spread randomly and did not allow for topical treatment.

### 2.2. Measurement techniques

#### 2.2.1. Spectral reflection analysis

A popular approach to remote sensing consists of analysing the reflected spectral radiation from the canopy (or single leaves) in order to find differences between healthy and infected plants. Diseases can be mainly detected as a stress: this means a higher yellow-red reflectance (due to lower pigmentation and chlorophyll content) and a lower NIR reflectance (due to the structural collapse of the dying cells), Fig. 2. This confirms visual observations in which a necrotic leaf area seems more yellow-brown.

#### 2.2.2. Hyperspectral imaging

The working principle of the fibre optic spectrograph (FOIS) is very similar to that of the Line Imaging Spectrograph (LIS) and is illustrated in Fig. 3. As LIS has a line as Field of View (FOV), called the Line of View (LOV), FOIS is built in such a way that it looks like a spectroradiometer with a circular FOV (COV). The light from the COV is conducted to the prism-grating-prism element using optical fibres through separate entrance slits. Ultimately separate spectra are collected from the different fibres on discrete zones of the CCD.

A multitude of optical fibres (15 in total) were arranged along the length of the boom and each fibre was pointed downwards, collecting light from an area of about 20 cm

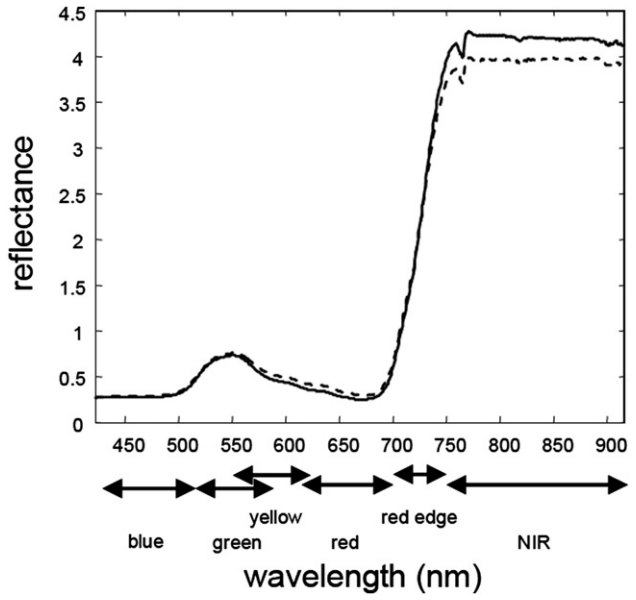


**Fig. 2 – Intensity normalised reflectance spectra for greenhouse septoria leaf blotch presence; the X-axis represents the wavelength region in nm, the Y-axis is the reflectance (dimensionless). The continuous line spectrum corresponds to healthy leaves while the dotted line corresponds to diseased leaves.**

diameter at upper canopy level. The fibres then guide the light to a spectrograph. The incoming light is collected using 16 optical fibres, one of which is used as an ambient light reference. The fibres are connected to the input aperture slit of the Specim V9 spectrograph's. The spectrograph output is imaged with a Leutron LV-1000 monochromatic CCD camera with a resolution of 1300 × 1030. To compensate for the dark level caused by the camera, an automatic shutter was fixed in front of the camera. Data was collected with a Leutron PicPort-Stereo-H4S frame grabber card. Sixteen spectra are imaged on the camera's sensor surface. From the image plane, the spectra are saved after averaging adjacent pixels.

### 2.2.3. *Multispectral imaging*

A CIR (Colour Infrared) camera was used to obtain high resolution data from the field. The camera objective was Nikon 24/2.8 giving about 1 × 2 m image area in the canopy level. Thus only a small portion of the boom width could be analysed. The camera selected was a Duncantech MS4100-CIR, having a resolution of 1920 × 1080 pixels. The wavelength channels of the camera were: green centre 550 nm, bandwidth 40 nm; red 660 nm, bandwidth 40 nm; and NIR 800 nm, bandwidth 65 nm. The data were collected on a PC using a National Instruments PCI-1428 frame grabber board.

Foliar disease infections can be seen as a spatial pattern on the leaf. Therefore one could opt for imaging systems. A crucial problem here is how to identify a disease spot. Mostly no illumination references are available during imaging and ambient conditions change drastically. These methods should thus rely on relative changes in image features that appear when monitoring the same plant. Specifically, this means that, for every acquired image, algorithms are needed to discriminate leaf from soil and to locate possible disease lesions.

All filters and thresholds used are not solely dependent on ambient conditions, but are also related to the acquisition circumstances (lens aperture, camera gain settings, CCD exposure time, etc). Fig. 4 shows a Colour Infrared (CIR) image (in false colour) with the subsequent processed image.

An algorithm based on monochromatic sub-images acquired at 675 nm (red region) and 750 nm (NIR region) was designed and implemented in two operational steps. First,

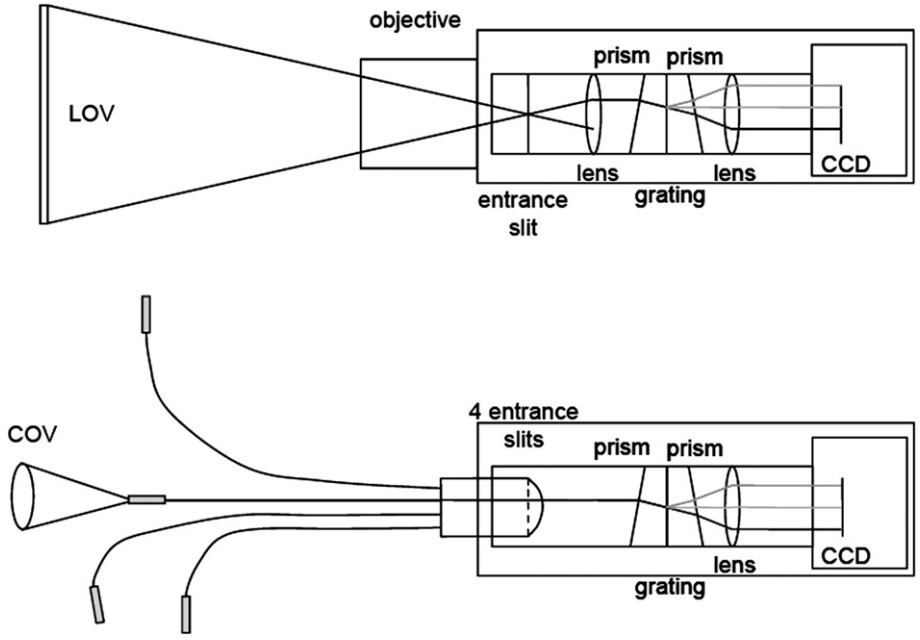


**Fig. 3 – Schematic of the working principle of a LIS (above) and FOIS (under).**

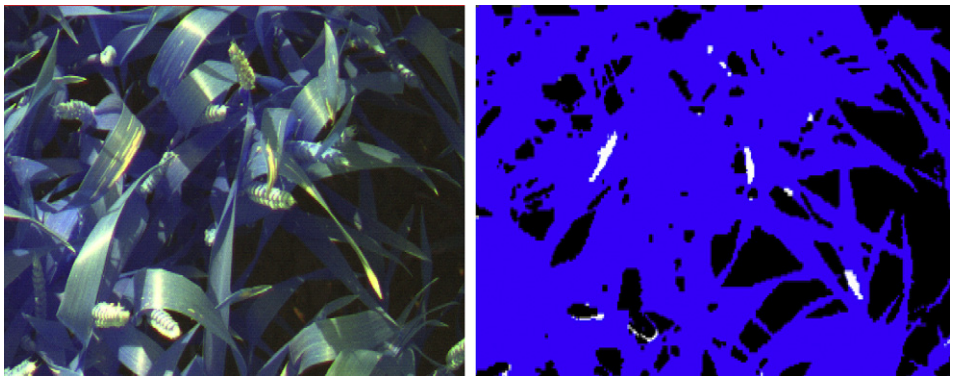

**Fig. 4 – On the left: a raw CIR image where the blue colour represents a NIR waveband, red and green colours represent respectively red and green wavebands; on the right: the resulting lesion map with classified pixels as lesions in white and as healthy vegetation in blue.**

pixels were discriminated in two classes, vegetation and background soil, based on their grey levels in 675 nm and 750 nm sub-images; secondly, discriminated vegetation pixels were classified as healthy tissue or lesions basing on their 675 nm grey levels. Output of the analysis procedure is a lesion index (LI) which quantifies the fraction of the imaged vegetation classified as lesions.

Given two monochromatic sub-images, $I_{675}(x,y)$ and $I_{750}(x,y)$, where (x,y) represents the pixel coordinates, a normalised difference vegetation image $I_{NDVI}(x,y)$ is calculated by applying pixel by pixel the following operator:

$$I_{NDVI}(x,y) = 1024 \cdot \frac{I_{750}(x,y) - I_{675}(x,y)}{I_{750}(x,y) + I_{675}(x,y)} \quad (1)$$

The $I_{NDVI}$ is a convenient transformation since changes in illumination intensity affect both wavebands in a similar way. Hence the grey levels in image $I_{NDVI}$ are robust against the large variations in light conditions occurring during outdoor measurements. Moreover, due to their spectral properties at these wavelengths, healthy vegetation, lesions and soil pixels had different grey levels in an $I_{NDVI}$ image. This was confirmed by the results of a manual pixel selection on a set of $I_{NDVI}$ images: high grey levels were obtained for healthy vegetation ($I_{NDVI}$ = 400–800, on 1024 scale) and low grey levels for lesions ($I_{NDVI}$ = 50–200, on 1024 scale) and soil ($I_{NDVI}$ = 100–300 on 1024 scale).

The more lesions that are observed, the higher the disease pressure. The proportion of leaf area showing lesions is called the lesion index (LI). A lesion index LI for the multi-spectral image was computed as:

$$LI = \frac{n_L}{n_L + n_H} \quad (2)$$

where $n_L$ represents the number of pixels corresponding to lesions and $n_H$ represents the number of pixels corresponding to healthy tissue. The index LI is finally assumed to represent the disease severity measured in the canopy area imaged.

Multispectral imaging provides an effective instrument for detecting lesions. The use of only one red and one NIR image is sufficient to separate a diseased area from healthy tissue. The fundamental question here is to relate the detected lesions with disease presence. Fig. 5 shows the relationship between the lesion index (LI), calculated for images acquired in different locations of two infected field plots, and the visual quantification of disease severity on the two upper leaves. The measurements refer to field plots infected with both yellow rust and septoria leaf blotch, the latter less heavily spread, at advanced disease stages.

### 2.2.4. *Disease detection stage*

The stage of infection at which the disease becomes detectable is clearly different between the presented methods. Using increased discolouration of infected leaves, the disease evolution can be monitored by spectral methods slightly before the first sporulation. Finally, when symptoms appear as obvious lesions, multi-spectral imaging becomes useful. For laboratory measurements on single plants, the precise

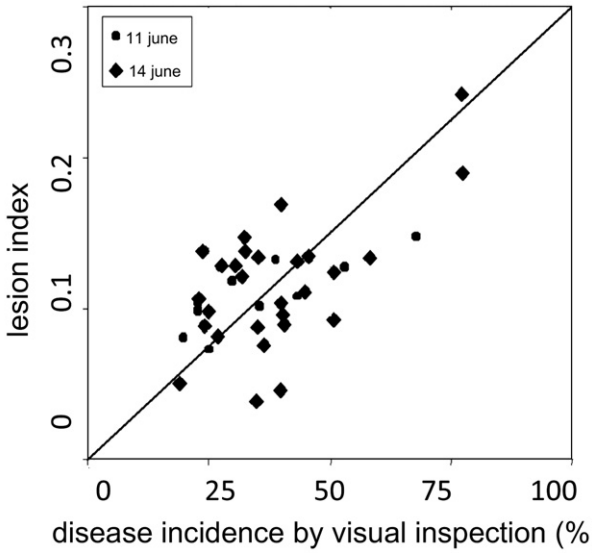


**Fig. 5 – Relationship between yellow rust and septoria leaf blotch severity reported by pathologist inspection in sampling locations and the LI calculated for multi-spectral images acquired in same locations of infected plots.**

date of infection can be critical, and pre-visual disease assessment might be necessary. In field circumstances, detection of diseases before sporulation provides the opportunity to prevent a new infection cycle. Lesions at that moment are already visible and highly infected plants will show advanced discolourations. Reflection-based systems should provide sufficient information for accurate mapping of diseases.

### 2.3. Data processing methods

#### 2.3.1. Waveband selection for yellow rust detection

For the waveband selection, a procedure similar to that of Moshou, Bravo, West et al. (2004) was used. The spectral resolution of the spectrograph was 18 nm because every 25 pixels were fused into larger bands of 18 nm using uniform averaging. In order to find the wavebands that best discriminated between areas diseased with yellow rust and healthy areas, wavebands were chosen through a stepwise variable selection. The procedure was based on the following: a waveband was only selected when its addition to the existing set of selected wavebands significantly increased the discriminating power of the new set of wavebands as determined by an F-test; and before a new waveband was chosen, the already chosen wavebands were investigated for the significance of their presence in the selected set. The ultimate selection was then used to build the discrimination model. The waveband selection leads to the advantage that only three wavebands need to be processed from each image, which reduces substantially the computational burden.

#### 2.3.2. Quadratic discriminant analysis (QDA) for yellow rust detection

Once the most discriminating set of wavebands was selected, a simple discrimination rule was defined. This criterion, called the quadratic classification rule, was based on the Mahalanobis distance of a single observation (average of normalised spectra over a fixed window) to the class means (healthy or diseased). An observation was then classified according to the smallest Mahalanobis distance to a class mean.

#### 2.3.3. Neural networks for yellow rust detection

Feed-forward neural networks (Rumelhart, Hinton, & Williams, 1986) provide a general framework for representing non-linear functional mappings between a set of input and output variables. Three layer networks (one hidden layer) are universal approximators. However, this does not directly impact the classification problem. In fact a Multi-Layer Perceptron (MLP) with two hidden layers carries the property of forming arbitrary decision surfaces which makes it a better candidate for complex classification problems.

For training, Bayesian regularisation (Bishop, 1995) was used. A validation set was used to test the generalisation performance of the neural network. The number of neurons in the input layer was equal to the number of wavebands used. The output layer had two neurons representing the two classes (healthy and diseased). Different numbers of neurons in the hidden layer were used, varying between 5 and 25 in steps of 5. Best results were obtained using a two hidden layer neural network with respectively 30 and 15 neurons, 26 inputs (25 spectral bands and LI) and two outputs (diseased-healthy). The hidden layers and the output layer of the MLP had sigmoid neurons. The training algorithm of Bayesian regularisation has the advantage of avoiding overtraining, hence improving generalisation performance. Other types of kernel functions like Radial Basis Function bases are not used with MLP hence they have not been included in the study. Adding more neurons in the hidden layer does not improve the generalisation result when Bayesian regularisation is used as the training algorithm, because weights that are not used remain small, and therefore the extra hidden neurons become inactive. Hence, the preferred neural network configuration was the one with the lowest complexity from the validated ones that did not compromise performance.

### 2.4. A disease detection prototype

In order to gather spatial data related to disease presence over an entire field, a prototype was assembled (Fig. 6). The general idaea behind this prototype is to combine two independent disease detection systems: a multi-spectral imager and a spectrophotometer by means of a multi-fibre spectrograph. While multi-spectral imaging provides a reliable idea of necrotic spot concentration on wheat leaves, the spectrophotometer will concentrate on the analysis of reflectance spectra measured at canopy level. The insertion of optical fibres on a spray boom offers the possibility to sample over the entire boom width. The acquisition of the optical data is synchronised with the accompanying DGPS positional data. The positioning data was collected with an Omnistar Trimble

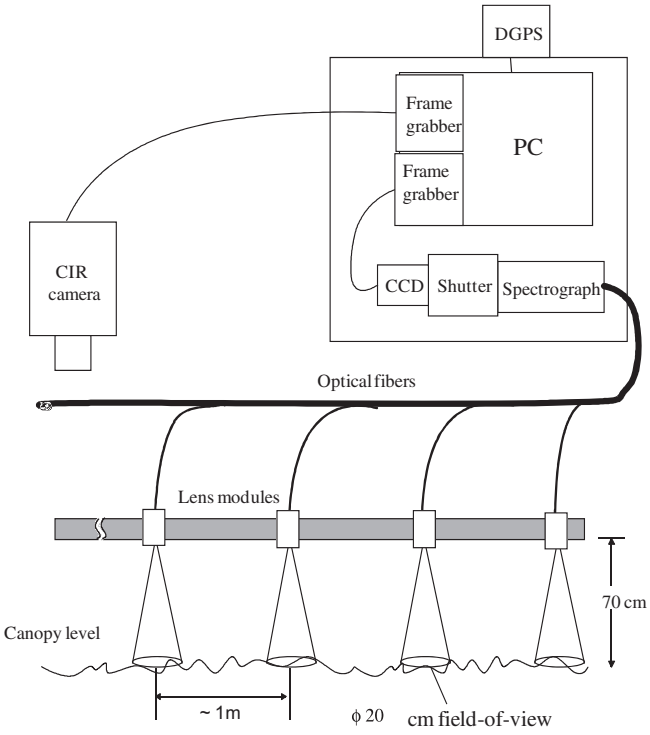


**Fig. 6 – Block diagram of the multi-sensor optical platform.**

7114 LR12 differential GPS-receiver. The DGPS was used to get spatial information for each optical measurement. The optical measurements were made with a constant time interval.

A multitude of optical fibres (15 in total) are arranged along the length of the boom and each fibre pointed downwards, collecting light from an area of about 20 cm diameter at the upper canopy level. The fibres then guide the light to a spectrograph. In the boom direction, fibres are spaced at 1 m intervals; in the driving direction, data should be acquired at maximum 1 m distances triggered by the on-board DGPS system independently of the tractor speed. The prototype used is illustrated in Fig. 7. The oscillations of the spray boom did not cause any difficulties because during the acquisition the tractor was stopped to take the measurements.

The final integrated prototype platform combining disease detection and disease management consists of the following components:

1. A disease detection system, based on optical sensors, mounted on a tractor spray boom that can differentiate between diseased and healthy areas of crop.
2. A tractor-mounted GPS system that can determine the position of the tractor in the field:
3. A computer-controlled spray boom system that can selectively operate spray nozzles.

## 3. Results and discussion

The inclusion of different fertilisation levels crossed with the two diseases assures the robustness of the classifier against variations due to different nitrogen content. The disease prototype has been tested only in the case of yellow rust because it appeared in patches so it allowed topical treatment. On the other hand septoria leaf blotch appeared to spread randomly and it did not allow for topical treatment.

### 3.1. *Sensor fusion results for yellow rust detection*

Sensor fusion is a method of integrating signals from multiple sources. Information received from multiple-sensors is processed using “sensor fusion” or “data fusion” algorithms. The feasibility of using sensor fusion for more robust and accurate detection of fungal diseases and nutrient stresses has been demonstrated by Moshou, Bravo, Oberti et al. (2005) and Bravo, Moshou, Oberti et al. (2004).

A general arrangement of the optical components of the prototype is shown in Fig. 6. From Fig. 7 it is more clear that the field of view of the multi-spectral camera coincides with the fields of view of two fibres. The features that were used for fusion, the LI from the multi-spectral camera and the average levels per spectral waveband, were obtained from the two fibres that have the same field of view with the multi-spectral camera. The other fibres were used for detecting foci of disease without the multi-spectral camera.

Sensor data fusion was performed by concatenating the LI resulting from the CIR camera to the average levels per spectral waveband from the two fibres. This was possible since the fibres below the CIR camera were concentrated in the field of view of the CIR camera. By combining the spectral wavebands with the LI, it is possible to estimate the classification efficiency due to fusion. Spectral data between 450 and 900 nm were divided into 25 10-pixel wide wavebands (covering 18 nm each) in order to remove as much of the spectral noise as possible. A total of 281 healthy and 141 diseased spectra were used with 70% randomly chosen for training and the rest used for testing. Two methods were compared: quadratic discrimination (QDA) vs. neural network (NN), which was a Multi-Layer perceptron (MLP) trained with Bayesian regularisation, using a two hidden layer neural network with respectively 30 and 15 neurons, 26 inputs (25 spectral bands and LI) or four inputs (three spectral bands following waveband selection and LI) and two outputs (diseased-healthy). The waveband index refers to one of the 25 wavebands with a width of 18 nm that span the spectral region 450–900 nm. The wavebands that resulted from the procedure of waveband selection were:

1. index 3 is the band centred at 495 nm with width 18 nm.
2. index 17 is the band centred at 747 nm with width 18 nm.
3. index 22 is the band centred at 837 nm with width 18 nm.

The error percentage (Table 1) expresses overall misclassification rate calculated as number of misclassified test samples (diseased misclassified as healthy and vice-versa) divided by their total number. Using LI alone, the error percentage for QDA was equal to 7.8% while with the inclusion

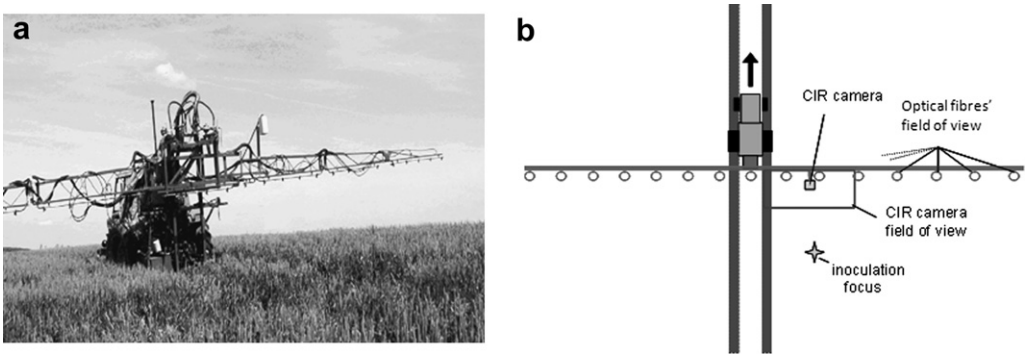


**Fig. 7 – (a) Picture of the tractor-mounted prototype platform. The field of view of the multi-spectral camera is on the right side of the tractor, 2 m away from the tramlines; the 15 downward looking spectrograph fibres are distributed along the boom frame, at 1 m distance from each other; (b) sketch of the instrumental arrangement.**

**Table 1 – Results of disease detection for yellow rust when using different classifiers. The lesion index has been used in all cases, and, except for the first line, was combined with spectral features as indicated in the waveband column.**

| Fusion classifier | Wave band index | Error percentage |
|---|---|---|
| QDA | No spectral features | 7.8 |
| QDA | 3 17 22 | 6.6 |
| NN | 3 17 22 | 5.9 |
| QDA | All 25 | 8.6 |
| NN | All 25 | 5.1 |

of three spectral features the error percentage dropped to 6.6%. The training of NN with LI and the three spectral features gave an improved error percentage of 5.9% compared to QDA. The best results were obtained by an NN which was trained with all wavebands and LI which gave an error percentage of 5.1%. This is a single trial, which makes it difficult to conclude that one approach will always be best.

What is noticeable from Table 1 is that the addition of all spectral features to LI has worsened the result in the case of QDA which gave an error percentage of 8.6% compared to the 6.6% when using only three spectral features together with LI. In the case of NN the addition of all spectral features to LI gave an error percentage of 5.1% which is a substantial improvement over 5.9% when using only three spectral features with LI. The results favour the NN over QDA because a two hidden layer MLP can form arbitrary decision surfaces depending on the number of nodes. It is important to note that QDA gets confused by the more complex decision regions that the extra features impose and hence gives worse results when all the wavebands are used. In the case of MLP the inclusion of more features gives a better result since it can handle the increased complexity of the decision regions.

### 3.2. *Site-specific spraying strategy for yellow rust*

The possibility that a link could be established between sensing yellow rust presence and the production of a site-specific spray command for treatment was investigated. The optical system developed must fit into a complete set of tools that allow site-specific treatment of in-field foliar diseases. The following is an example of how the disease detection results for yellow rust could be implemented into a practical spraying decision. The yellow rust disease detection results obtained from the multi-sensor prototype were used to construct a map (Fig. 8). The measured area corresponds to the plots (R4, R7 and R8; Fig. 1) that were inoculated with yellow rust spores. The grey dots are positions of measurements estimated as healthy and the black dots represent the field points estimated as diseased.

For radially propagated diseases like yellow rust, it is possible to determine a perimeter around a detected infection hazard using advanced epidemiological models. These models consider the disease presence above the detection

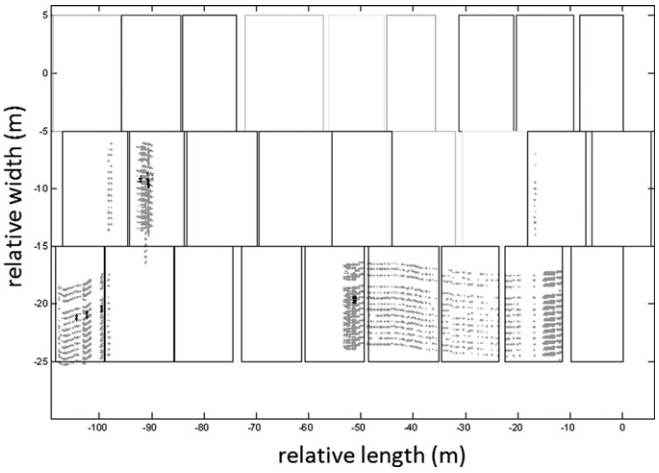


**Fig. 8 – Map with all optical observations in grey and detected yellow rust disease in black; data measured on June 6th, 2003.**

threshold at the moment of detection and therefore estimate real disease presence. By combining this presence with meteorological data, the models provide a minimal protection radius around the initially detected infection hazard. As it is impossible to estimate this effective presence during measurement, a two way approach is proposed:

1. Determining the location of diseases during an early field operation such as fertilisation.
2. Performing site-specific spraying when the effective disease presence is known following epidemiological analysis.

Although this approach assumes the presence of a mobile unit as a carrier of the prototype and an application mobile unit carrying out an independent sequential operation, a real-time approach where the two mobile units are considered as cooperating units also seems promising. The feasibility of such a field operation approach, in terms of operational planning, has already been demonstrated and proven. The operational planning for the inspection unit can be incorporated in any deterministic planning method. The planning for the application unit can be considered as a dynamic vehicle routing problem (Bochtis & Sørensen, 2010), where there is no *a priori* information and thus the information that is needed for the generation of a set of feasible routes and missions is dynamically revealed to the decision-making system, or as a vehicle routing problem with stochastic demands (Bochtis & Sørensen, 2009), where the demand for fungicide at each location is unknown at the time of planning, but it is assumed to follow a known probability distribution, probably derived from historical data.

Actual spray recommendation maps were constructed from disease detection data using the multi-sensor prototype presented above similar to the procedure presented in West et al. (2003). The data concerning yellow rust were measured on June 6th, 2003. It was detected at a 5% infestation threshold. The occurrence of false positives was not taken

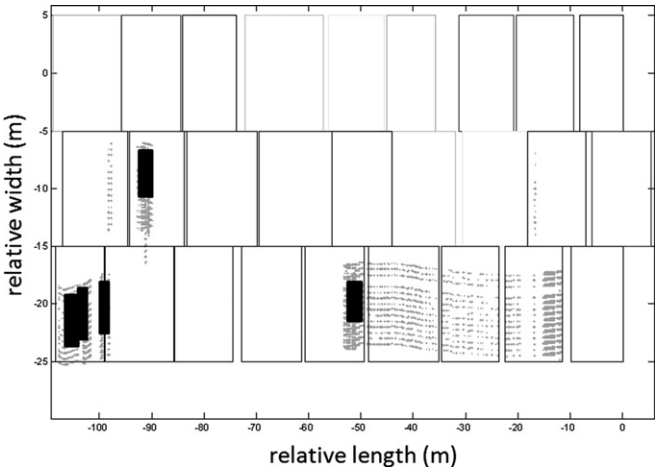


**Fig. 9 – Spray recommendation map based on a 3 m protection distance. The estimation of at - risk areas was made on the observation date.**

into account since all the detected foci were actually infected. The disease pattern in the field was optically detected and mapped (Fig. 8). The disease map was used, together with relevant information (e.g., growth stage and uppermost-infected leaf) to make a spray decision using the decision support system (DSS) Proculture (http://procultureweb.fymy.ucl.ac.be/) which has been presented in Moreau and Maraite (1999). The disease map consisted of rectangular "pixels" each representing the disease status for that area of the field. Each pixel was labelled as "diseased" or "healthy". If the decision to spray was made, then the disease map was transformed into a spray map that corrected for undetected disease and, if necessary, incubating disease. This information was corrected based on the fact that only 3 m sections of the boom could be turned on and off so that a spray recommendation map was obtained (Fig. 9).

The dark areas in Fig. 9 show the part of the measured area that needs to be treated following the spray recommendation. The grey areas show the part of the measured area that does not need fungicide protection. Taking into account that the field area that contained inoculated plants and could be scanned for disease presence corresponded to plots R4, R7 and R8 in Fig. 1, the total area that would have to be sprayed in the case of blanket application would be equal to 1350 $m^2$. The area that needs to be sprayed according to the recommendation map is approximately 70 $m^2$. This corresponds to 5.2% of the area that would have been sprayed in a blanket application. Around 450 $m^2$ have been actually scanned, therefore a more realistic calculation gives that 15.5% of the scanned area has to be sprayed. This result corresponds to circa 94.8% savings in pesticides compared to blanket application while the comparison to scanned area indicates an 84.5% savings in pesticides. Due to the patchy appearance of yellow rust, a high classification rate means that the primary patches have been identified with 100% confidence even if individual spectra were not, as a patch contains a mixture of healthy and diseased spectra. So, the algorithm should be robust enough in patch identification indicating a disease focus. The potential savings in pesticides could thus be significant and may justify the use of the proposed scheme.

## 4. Conclusions

The acquisition of spatially accurate disease data plus efficient processing has been shown to have the potential to support practical spraying decisions. A robust multi-sensor prototype integrating optical sensing, GPS and data processing was constructed and calibrated. An intelligent multi-sensor fusion decision system based on a neural network has been developed to predict the presence of diseases or plant stresses. The functionality of automatic disease sensing and detection devices has been demonstrated, providing the basis for a site-specific spraying strategy against fungal foliar diseases. Field tests were carried out to optimise the functioning of the multi-sensor disease detection device. Yellow rust disease data were processed for an automatic site-specific spraying strategy in winter wheat. The disease map, based on automated optical sensing and intelligent prediction, provided a spatially variable recommendation for spraying that could lead to substantial savings in pesticides, with financial and environmental benefits.

## Acknowledgements

This research has been partially funded by the OPTIDIS project EU-QLK5-CT99-01280. The OPTIDIS project was funded by the EU under the Quality of Life Programme–Framework V.

## REFERENCES

Bishop, C. M. (1995). *Neural networks for pattern recognition*. Oxford: Oxford University Press.

Bochtis, D. D., & Sørensen, C. G. (2009). The vehicle routing problem in field logistics part I. *Biosystems Engineering, 104*(4), 447–457.

Bochtis, D. D., & Sørensen, C. G. (2010). The vehicle routing problem in field logistics: Part II. *Biosystems Engineering, 105*(2), 180–188.

Bravo, C., Moshou, D., Oberti, R., West, J., McCartney, A., & Ramon, H. (December 2004). Foliar disease detection in the field using optical sensor fusion. *Agricultural Engineering International: The CIGR Journal of Scientific Research and Development*, VI. Manuscript FP 04 008.

Bravo, C., Moshou, D., West, J., McCartney, A., & Ramon, H. (2003). Detailed spectral reflection information for early disease detection in wheat fields. *Biosystems Engineering, 84*(2), 137–145.

Cui, D., Zhang, Q., Li, M., Hartman, G. L., & Zhao, Y. (2010). Image processing methods for quantitatively detecting soybean rust from multispectral images. *Biosystems Engineering, 107*(3), 186–193.

Devadas, R., Lamb, D. W., Simpfendorfer, S., & Backhouse, D. (2009). Evaluating ten spectral vegetation indices for identifying rust infection in individual wheat leaves. *Precision Agriculture, 10*(6), 459–470.

Huang, W., Lamb, D. W., Niu, Z., Zhang, Y., Liu, L., & Wang, J. (2007). Identification of yellow rust in wheat using in-situ

spectral reflectance measurements and airborne hyperspectral imaging. *Precision Agriculture, 8*(4–5), 187–197.

Lee, W. S., Alchanatis, V., Yang, C., Hirafuji, M., Moshou, D., & Li, C. (2010). Sensing technologies for precision specialty crop production. *Computers and Electronics in Agriculture, 74*(1), 2–33.

Moreau, J. M., & Maraite, H. (1999). Integration of knowledge on wheat phenology and Septoria tritici epidemiology into a disease risk simulation model validated in Belgium. *Aspects of Applied Biology, 55*, 1–6.

Moshou, D., Bravo, C., Oberti, R., West, J., Bodria, L., McCartney, A., et al. (2005). Plant disease detection based on data fusion of hyper-spectral and multi-spectral fluorescence imaging using Kohonen maps. *Real Time Imaging Journal-Special Issue on Spectral Imaging II, 11*(2), 75–83.

Moshou, D., Bravo, C., West, J., McCartney, A., & Ramon, H. (2004). Automatic detection of "yellow rust" in wheat using reflectance measurements and neural networks. *Computers and Electronics in Agriculture, 44*(3), 173–188.

Muhammed, H. H., & Larsolle, A. (2003). Feature vector based analysis of hyperspectral crop reflectance data for discrimination and quantification of fungal disease severity in wheat. *Biosystems Engineering, 86*(2), 125–134.

Naidu, R. A., Perry, E. M., Pierce, F. J., & Mekuria, T. (2009). The potential of spectral reflectance technique for the detection of Grapevine leafroll-associated virus-3 in two red-berried wine grape cultivars. *Computers and Electronics in Agriculture, 66*(1), 38–45.

Rumelhart, D. E., Hinton, G. E., & Williams, R. J. (1986). Learning internal representations by error propagation. In D. E. Rumelhart, & J. L. McClelland (Eds.), *Parallel distributed processing (part 1)* (pp. 318–362). Cambridge, USA: MIT Press.

West, J. S., Bravo, C., Oberti, R., Lemaire, D., Moshou, D., & McCartney, H. A. (2003). The potential of optical canopy measurement for targeted control of field crop diseases. *Annual Review of Phytopathology, 41*, 593–614.

Zhang, L., & Dickinson, M. (2001). Fluorescence from rust fungi: a simple and effective method to monitor the dynamics of fungal growth *in planta*. *Physiological and Molecular Plant Pathology, 59*(3), 137–141.

Zhang, M., Qin, Z., Liu, X., & Ustin, S. L. (2003). Detection of stress in tomatoes induced by late blight disease in California, USA, using hyperspectral remote sensing. *International Journal of Applied Earth Observation and Geoinformation, 4*(4), 295–310.